RHEOLOGICA ACTA

AN INTERNATIONAL JOURNAL OF RHEOLOGY

Vol. 20 | September/October 1981 | No. 5

Original Contributions · Originalarbeiten

Rheol. Acta **20**, 419 – 432 (1981)

ISSN 0035-4511 / ASTM-Coden: RHEAAK

Laboratory for the Technology of Macromolecular Compounds, Delft University of Technology

Simultaneous measurement of transient stress and flow birefringence in one-sided compression (biaxial extension) of a polymer melt

J. A. van Aken and *H. Janeschitz-Kriegl*

With 16 figures and 2 tables

(Received May 11, 1981)

Summary

Investigation of time dependent behaviour of a polystyrene melt is carried out with the aid of a new apparatus for biaxial extension. Use is made of the method of two impinging fluid streams guided by lubricated trumpet shaped metal walls. The flow birefringence is measured in the plane of symmetry and, at the same time, the force is measured which tends to separate the trumpets. The linear stress-optical relation turns out to be valid in this new flow geometry. An accurate value for the stress-optical coefficient can be determined from the relaxation experiments. The stress build-up as calculated from the optical measurements, is compared with the pertinent result of the theory of linear viscoelasticity. For the desired interconversion of dynamic moduli use is made of the approximation by Schwarzl and Struik. The steady state measurements are checked by the results of the non-linear model of Acierno et al.

Zusammenfassung

Eine Untersuchung des zeitabhängigen Verhaltens einer Polystyrolschmelze wird mit Hilfe eines neuen Apparates für biaxiale Dehnung ausgeführt. Hierfür wird die Methode des Aufeinanderprallens entgegengesetzt gerichteter Ströme verwendet, die von geschmierten trompetenförmigen Metallwänden geleitet werden. Die auftretende Strömungsdoppelbrechung wird in der Symmetrieebene gemessen, während die Kraft bestimmt wird, die die Trompeten auseinanderzutreiben versucht. Die lineare spannungsoptische Regel erweist sich auch für die neue Strömungsgeometrie als gültig. Ein genauer Wert des spannungsoptischen Koeffizienten ergibt sich aus Relaxationsexperimenten. Der Spannungsaufbau, wie er aus den optischen Messungen berechnet wird, wird mit dem entsprechenden Ergebnis der linearen Theorie der Viskoelastizität verglichen. Für die erforderliche Umrechnung der dynamischen Moduln wird die Näherung nach Schwarzl und Struik verwendet. Die stationären Messungen werden mit Hilfe des nicht-linearen Modelles von Acierno u.a. überprüft.

Key words

Biaxial extension flow, uniaxial compression flow, stagnation flow, flow birefringence, polystyrene melt

1. Introduction

The flow birefringence technique is a very useful method for the investigation of rheological properties of polymeric systems. However, because the optical measuring method is an indirect one, one has to rely on the stress-optical rule. Until now the flow birefringence technique was applied to experiments for the detection of the shear stress and normal stress differences (1 – 3). These experiments corroborate the validity of the stress-optical rule over a wide range of shear rates.

For the optical measurements it is desirable to have a constant optical path length. In most of

the extensiometers the polymer is stretched. During this operation the thickness of the sample decreases and no constant optical path length is available. By using a type of stagnation flow one has a polymer flow without instabilities. At the same time a constant optical path length through the sample can be realized. For such a stagnation flow the authors succeeded in developing an apparatus in which the optical and mechanical measurements can be carried out simultaneously. A description of this stagnation flow apparatus has recently been published (4). In the present paper further investigations of the velocity profile and of the force transducer are treated first. In this stagnation flow apparatus the time dependent behaviour of a polystyrene melt is measured both optically and mechanically.

The transient optical and mechanical measurements are carried out simultaneously at several temperatures and extension rates. To compare the measured and the theoretically expected extensional viscosity use has been made of the approximation of Schwarzl and Struik (5). This method, which predicts the stress-build-up of a linear viscoelastic fluid from the frequency dependencies of its dynamic shear moduli, is described among others by Gortemaker (3) in this thesis for shear experiments.

To describe the flow behaviour in the steady state in an extended range of strain rates, one may use a non-linear constitutive equation. Wagner proposed an integral type equation introducing a damping function (6). This method has been very successful in the description of the flow behaviour of polymer melts. Another successful method is given by the theory of Acierno and cooperators (7–9). The latter authors deal with a differential type of equation. Wagner's as well as Acierno's theories have been rather successful also in the description of flow birefringence data (11, 14). In the present paper the steady state flow behaviour will be described with the Acierno theory because the differential equations are easier to be handled.

2. Theory

2.1. Results of linear theory

As is well known, the results of the linear theory of visco-elasticity are applicable if the total strain is small or if the strain rate is small. For the "stressing" experiments described in this paper this means that linear behaviour can be expected just after the moment when the constant rate of extension $\dot{\varepsilon}$ is applied. Deviations from this linear behaviour are only expected when, after some time, the cumulated strain $\varepsilon = \dot{\varepsilon} t$ surpasses a certain value (of the order of unity for polymer melts). Only with a sufficiently small value of $\dot{\varepsilon}$ the whole time dependence of the "stressing viscosity" (viz. of the tensile stress divided by $\dot{\varepsilon}$) can be described with the aid of the linear theory. This is of importance since linear visco-elastic functions can mutually be interconverted. The mentioned stressing viscosity, for instance, can be calculated from the dynamic shear moduli G' and G'' as function of circular frequency. In this way the internal consistence of the results can be checked.

In particular, for the linear case one has

$$3\sigma_{21} = \sigma_t \qquad [2.1]$$

where σ_{21} is the shear stress at a value of the shear rate $\dot{\gamma}$ which coincides with the value of the extension rate $\dot{\varepsilon}$ at which the tensile stress σ_t is measured. Gortemaker showed in his thesis (8) that an application of the interconversion method of Schwarzl and Struik (5) to Lodge's equations enables us not only to calculate the build-up of the shear stress but also of the first normal stress difference as functions of time from the dynamic moduli $G'(\omega)$ and $G''(\omega)$ as functions of circular frequency ω.

In the case of extensional flow, however, the tensile stress takes over the role of the shear stress (see eq. [2.1]). No analogon to the first normal stress difference of the shear experiment is found. Consequently, we can dismiss Lodge's equations and simply use the classical linear theory. According to this theory the storage modulus $G'(\omega)$, the loss modulus $G''(\omega)$ and the shear stress build-up $\sigma_{21}(t)$ can be expressed in terms of the relaxation time spectrum $H(\tau)$ by the following equations:

$$G'(\omega) = \int_{-\infty}^{+\infty} H(\tau) \frac{\omega^2\tau^2}{1 + \omega^2\tau^2} d\ln\tau \qquad [2.2]$$

$$G'' = \int_{-\infty}^{\infty} H(\tau) \frac{\omega\tau}{1 + \omega^2\tau^2} d\ln\tau \qquad [2.3]$$

$$\sigma_{21}(t) = \dot{\gamma} t \int_{-\infty}^{\infty} H(\tau) \frac{1 - e^{-t/\tau}}{t/\tau} d \ln \tau . \qquad [2.4]$$

Schwarzl and Struik called the functions occurring in these integrals behind $H(\tau)$ "intensity functions". They developed a method for the linear approximation of the intensity function of eq. [2.4] in terms of the intensity functions of eqs. [2.2] and [2.3], putting $t/\tau = 1/\omega\tau$. From the maximum deviation of this approximation from the real intensity function they could derive the maximum error of their conversion formula. Gortemaker derived in this way for the shear stress build-up the equation:

$$[\sigma_{21}]_t = \dot{\gamma} t [G'(\omega) - 0.322\, G''(\omega/2) + 0.580\, G''(2\omega)]_{\omega = 1/t} . \qquad [2.5]$$

The relative maximum error in this equation is $\pm 5.5\%$.

Because the tensile stress build-up $\sigma_{11}(t)$ at sufficiently low $\dot{\varepsilon}$ has the same time dependence, the following relation can be used:

$$[\sigma_{11}]_t = 3\dot{\varepsilon} t [G'(\omega) - 3.22\, G''(\omega/2) + 0.580\, G'(2\omega)]_{\omega = 1/t} . \qquad [2.6]$$

The relaxation after reaching the steady state is given by:

$$\left[\frac{\sigma_{11}}{\dot{\varepsilon}}\right]_t^r = \left[\frac{\sigma}{\dot{\varepsilon}}\right]_{t=\infty} - \left[\frac{\sigma}{\dot{\varepsilon}}\right]_t . \qquad [2.7]$$

2.2. Non-linear viscoelastic model

In this section the non-linear viscoelastic model of Acierno et al. will be treated. This theory is formulated in terms of an approximate line spectrum of relaxation times. The contributions of the separate relaxation processes are summed up. The following equations are needed to describe the behaviour of a polymeric melt:

$$\boldsymbol{\sigma} = \sum_i \boldsymbol{\sigma}_i , \qquad [2.8]$$

$$\frac{1}{G_i}\boldsymbol{\sigma}_i + \tau_i \frac{\partial}{\partial t}\left(\frac{1}{G_i}\boldsymbol{\sigma}_i\right) = 2\tau_i \boldsymbol{D} , \qquad [2.9]$$

$$G_i = G_{0i} x_i ; \qquad \tau_i = \tau_{0i} x_i^{1,4} , \qquad [2.10]$$

$$\frac{dx_i}{dt} = \frac{1}{\tau_i}(1 - x_i) - \alpha x_i \frac{1}{\tau_i} \sqrt{\frac{E_i}{G_i}} . \qquad [2.11]$$

In these equations as separately valid for every relaxation mechanism, $\boldsymbol{\sigma}_i$ is the stress tensor increment, G_{0i} the linear relaxation modulus, τ_{0i} the linear relaxation time and $1 \geq x_i \geq 0$ an internal structural parameter. Dimensionless parameter α is, in general, adjusted by fitting the steady non-Newtonian shear viscosity as a function of shear rate. It should be of the order of unity and essentially the same for all types of polymers.

The symbol $\boldsymbol{D}$ stands for the rate of strain tensor:

$$\boldsymbol{D} = \tfrac{1}{2}(\nabla \boldsymbol{v} + \nabla \boldsymbol{v}^{\mathrm{T}}) \qquad [2.12]$$

whereas E_i is the contribution to the elastic energy associated with the i-th relaxation time:

$$E_i = \tfrac{1}{2} \operatorname{tr} \boldsymbol{\sigma}_i . \qquad [2.13]$$

For steady uniaxial extensional flow the velocity components are:

$$\left.\begin{aligned} v_1 &= \dot{\varepsilon} x_1 , \\ v_2 &= -\tfrac{1}{2}\dot{\varepsilon} x_2 , \\ v_3 &= -\tfrac{1}{2}\dot{\varepsilon} x_3 \end{aligned}\right\} \qquad [2.14]$$

in which $\dot{\varepsilon}$ is the extension rate. The 1-direction is the direction of extension, the 2- and 3-directions are perpendicular to the 1-direction and to each other.

In the steady state eqs. [2.9] with [2.12] and [2.14] gives

$$\left.\begin{aligned} \frac{\sigma_{11,i}}{G_i} &= \frac{2\tau_i \dot{\varepsilon}}{1 - 2\tau_i \dot{\varepsilon}} , \\ \frac{\sigma_{22,i}}{G_i} &= -\frac{\tau_i \dot{\varepsilon}}{1 + \tau_i \dot{\varepsilon}} , \end{aligned}\right\} \qquad [2.15]$$

and since $\sigma_{22,i} = \sigma_{33,i}$, E_i becomes

$$E_i = \tfrac{1}{2}\sigma_{11,i} + \sigma_{22,i} . \qquad [2.16]$$

Eq. [2.11] can now be written for the steady state as:

$$(1 - x_i) = \alpha x_i \left(\frac{\sigma_{11,i}}{2G_i} + \frac{\sigma_{22,i}}{G_i}\right)^{1/2} = 0 . \qquad [2.17]$$

Insertion of the two eqs. [2.15] into [2.17] enables us to calculate the internal structural

parameter x_i, if the linear relaxation time τ_{0i}, the extension rate $\dot{\varepsilon}$ and the adjustable parameter α are known. The viscosity as a function of the extension rate can then be calculated with $G_i = G_{0i}x_i$ from

$$\eta_e = \sum_i \eta_{e,i} = \sum_i \frac{\sigma_{11,i} - \sigma_{22,i}}{\dot{\varepsilon}} . \qquad [2.18]$$

3. Further improvements of the experimental technique

3.1. Lubrication

For an incompressible fluid an ideal stagnation flow, as drawn in figure 1, is confined by the imaginary surface:

$$zR^2 = \text{constant} = A . \qquad [3.1]$$

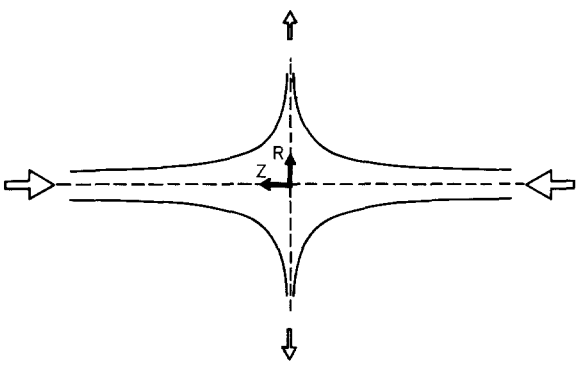

Fig. 1. The ideal stagnation flow of two impinging streams. The equation of the stream lines in cylindrical coordinates is zR^2 = constant

In cylindrical coordinates the velocity components are given by

$$v = \left(\dot{\varepsilon}_z z, -\frac{\dot{\varepsilon} z}{2} r, 0\right) \qquad [3.2]$$

in which $\dot{\varepsilon}_z$ is negative. However, as no confusion can arise in the present context, the value of $\dot{\varepsilon}_z$ will be quoted in this paper simply as $\dot{\varepsilon}$. From eq. [3.2] we learn that, in the ideal case, all fluid particles at a given distance $z = z'$ from the plane of symmetry have the same velocity in the axial direction and all particles at a distance $r = r'$ have the same velocity in the radial direction. However, if over a certain distance $(z_1 - z_2)$ along the z-axis (with $z_1 \gg z_2$, see previous publication) the fluid is confined by a solid surface according to eq. [3.1], the velocity components given by eq. [3.2] will be valid only approximately (15). It should also be kept in mind that the melt enters the diverging (trumpet shaped) areas on either side of the plane of symmetry through cylindrical ducts and leaves this area through the clearance between the opposite rims of the trumpets (which are carved into outwardly cylindrical parts). In order to avoid the build-up of considerable tangential stress at the confining surfaces one has to arrange for an effective lubrication layer between the melt and the wall. Because the quality of the lubrication layer was throught to be essential for the desired plug flow of the melt, the velocity profile in the melt was examined.

First, however, the alignment of the apparatus and the equality of the speeds of the pistons were checked by the use of differently coloured polystyrenes at either side of the plane of symmetry. In figure 2 a sample, as obtained after the disassemblage of the unit is shown. Due to the normal stress the material expands when it leaves the ringshaped gap. Both coloured streams appear to have remained on their own side of the plane of symmetry. This means that the speed of the pistons and the velocity profiles in both parts are the same.

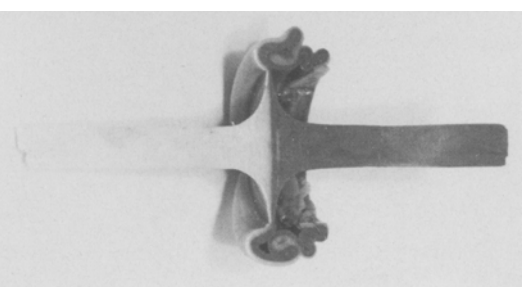

Fig. 2. This figure shows a cross-section of a polystyrene sample which was strained in the apparatus for a short time. To check the alignment of the apparatus differently coloured polystyrene samples were used on either side of the plane of symmetry

In order to examine the influence of the lubrication on the mechanical and the optical measurements and on the velocity profile itself experiments were carried out under the following conditions:

a. Lubrication with silicone oil (viscosity 10^3 Pa.s at 170°C).

b. No lubrication at all.

Both types of experiments were carried out at the same temperature (170°C) and with the same set of nominal extension rates, viz.: $\dot{\varepsilon} = -3.6 \cdot 10^{-3}\ s^{-1}$ and $-9.6 \cdot 10^{-3}\ s^{-1}$.

a. Lubrication with silicone oil.
In the cylindrical stems of two transparent polystyrene samples some slices of coloured polystyrene were placed. These samples were treated with silicone oil in the usual way and put into the unit. After these samples were heated up, the melt was pushed forward by the pistons for a short time. After cooling down, the samples were removed from the unit and cut along their axis in two halves (fig. 3). In the centre of the sample the coloured layers were found to be still nearly flat. Only close to the wall the coloured material was smeared out over a certain axial distance. This means that in the centre the velocity gradient is rather small and that a high gradient is found only along the wall. The conclusion is that by the lubrication with this silicone oil a rather good approximation of a plug flow is created.

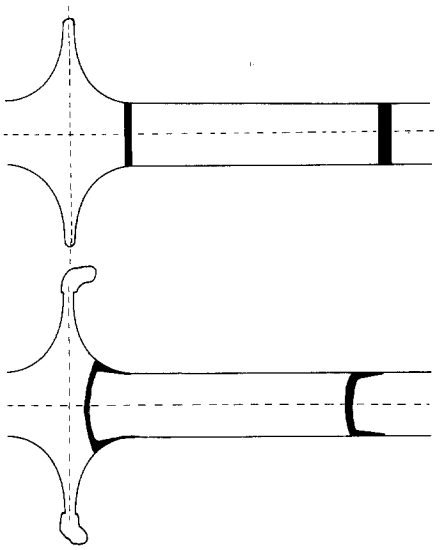

Fig. 3. The velocity profile in the sample is made visible by the thin black slices of polystyrene. The upper figure gives the position of the slices before the apparatus is started. The sample was treated during 30 s at 150 °C: The value of extension rate was $\dot{\varepsilon} = -3.6 \cdot 10^{-3}\ s^{-1}$

b. Experiments without lubricant.
The apparatus was carefully cleaned from silicone oil before these experiments were started. Some coloured material was put between the tip of the piston and the sample. As expected, the melt stuck to the wall. In the cylindrical part of the duct the material was scraped from the wall by the piston. As a consequence, after a few seconds the coloured material was transported from the end of the sample through the centre to the stagnation point. The actual extension rate in the centre of the sample was apparently much higher than the calculated nominal extension rate. The force which tends to separate the two trumpets, was found to be about ten times as high as in the lubricated case. Also the optical measurements were inadmissibly influenced by this no-slip condition at the wall

One the conclusions, which can be drawn from these experiments, is that the quality of the lubrication layer is of a much lower influence on the optical measurements than it is on the mechanical measurements. An explanation is that the optical measurements are carried out with the aid of a light beam passing through fluid layers very close to the plane of symmetry. In the direct environment of this plane a rather good approximation of a flat velocity profile is obtained. The force measurements, however, are certainly influenced by the resistiance against radial flow, as caused for a great deal by the friction at the wall. In fact, as a consequence of this resistance a non-uniform distribution of the hydrostatic pressure is created over the cross-section in the central plane. This distribution, which possesses a maximum at $r = 0$ is superimposed on the uniform normal stress $-\sigma_{11}$, which is expected as a consequence of the desired velocity field (see eq. [3.2]). This results in an undesired increase of the total separation force, as measured in the present apparatus.

3.2. Calculation of the normal stress from the force measurements

As just indicated, the value of the normal stress $\sigma(= -\sigma_{11})$ must be deduced from the axial separation force as measured on one of the trumpets (for shortness called "cylinders", because of their outside appearance). This force is continuously recorded on paper as a function of time. As described in the preceding section, the measured force has to be corrected for non-ideal lubrication. Assuming for simplicity that the non-ideal lubrication causes a parabolic top on the flat pressure profile, we can use a correction based on measurements with a divided cylinder (i.e. a cylinder consisting of two slidingly fitting concentric parts so that the separation force can be measured alternatively over the whole cross-section and over the smaller cross-section of the inner cylinder). This method is described in the preceding paper (4). The pertinent correction equation reads:

$$\frac{\sigma}{\sigma_1} = 1 + \frac{1}{1 - \left(\frac{R_2}{R_1}\right)^2}\left(1 - \frac{\sigma_2}{\sigma_1}\right) \qquad [3.3]$$

where σ_1 is the average pressure over the whole area with radius R_1, σ_2 is the average pressure

over the inner (smaller) area with radius R_2 and σ is the rim pressure which should be identical with the normal stress $-\sigma_{11}$.

In the standard equipment we have $R_1 = 10$ mm and $R_2 = 6.5$ mm. It was necessary to use the construction with the divided cylinders each time because no reproducible relation between the correction factor and the temperature or extension rate $\dot{\varepsilon}$ could be found, although the precedure of lubrication of the samples and cylinders was always the same. The correction factor σ/σ_1 lies between 0.6 and 0.8. In order to justify the assumption of the parabolic top on the pressure profile inner cylinders of different radii R_2 were used, viz.: $R_2 = 5.5$; 6.5 and 8.0 mm. This experiment failed, as for every ratio R_2/R_1 a new sample had to be used: apparently the lubrication layer was not always of the same quality.

A disadvantage of this type of lubrication is that the lubrication layer is pressed out of the cylinders together with the melt. During these processes a reduction of the layer thickness takes place as soon as the layer enters the trumpet shaped part of the cylinder. The addition of extra lubrication oil at the beginning of the trumpet shaped part through holes in the wall will be of some extra influence on the mechanical measurements since over-pressure must be applied. Let us hope that the use of coated cylinders will solve this problem and bring about a considerable simplification of the preparation of the samples.

3.3. The temperature measurement

In contrast to the procedure followed with the measurements shown in the previous paper (4), the precise temperature of the melt is presently found by the subsequent insertion of a thermocouple into the centre of the gap. This temperature appears to differ from the one measured with the aid of a thermocouple located in a slot in the outer surface of the metal cylinder.

4. Characterization of the sample

The polymer used in this experiment was a technical polystyrene of Hoechst (Hostyren N 4000 V). This polymer was chosen because an extensive rheological characterization was available from the work by Gortemaker, who used this polystyrene in his shear experiments. Various averages over the relative molecular mass distribution of the polystyrene as obtained from GPC measurements, are according to ref. (3):

$M_n = 8700$, $M_w = 240000$,
$M_z = 495000$, $M_{z+1} = 832000$.

The storage and loss moduli G' and G'' as functions of the circular frequency ω were obtained with the aid of the automatic dynamic viscometer, designed by Te Nijenhuis at this laboratory. The values of $G'(\omega)$ and $G''(\omega)$ were measured at a series of different temperatures. Master curves are constructed over an extended range of frequencies with the aid of the time-temperature superposition principal (fig. 4). As reference temperature T_0 a temperature of 170 °C was chosen. In this procedure $G'(\omega)$ and $G''(\omega)$ are reduced to $G_r' = G' \frac{\rho_0 T_0}{\rho T}$, where T is the temperature of the measurement in K and ρ is the pertinent temperature dependent density. The shift factor a_T is given in figure 5. It is in agreement with the WLF-equation (see Gortemaker et al. (10)).

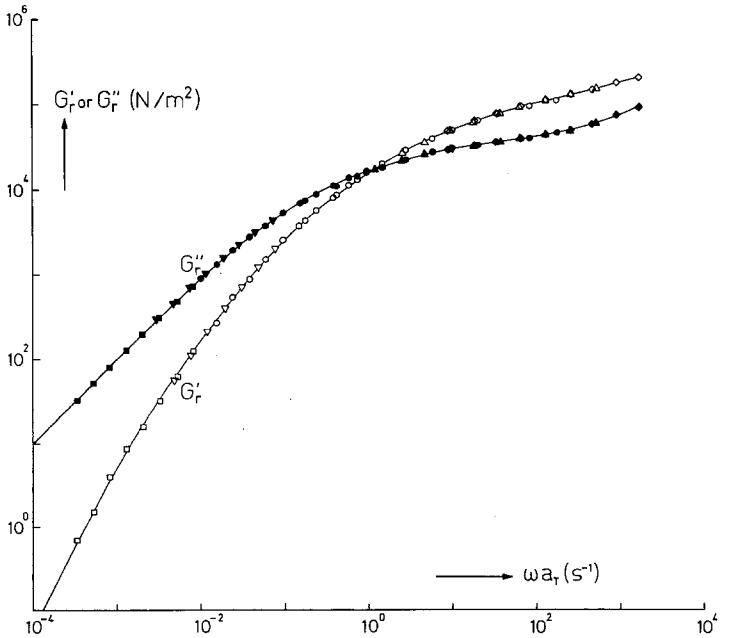

Fig. 4. Double logarithmic plot of the reduced storage modulus $G_r' = G' \frac{\rho_0 T_0}{\rho T}$ (open symbols) and loss modulus $G_r'' = G'' \frac{\rho_0 T_0}{\rho T}$ (filled symbols) versus ωa_T for Hoechst PS at 170 °C (see Gortemaker (3))

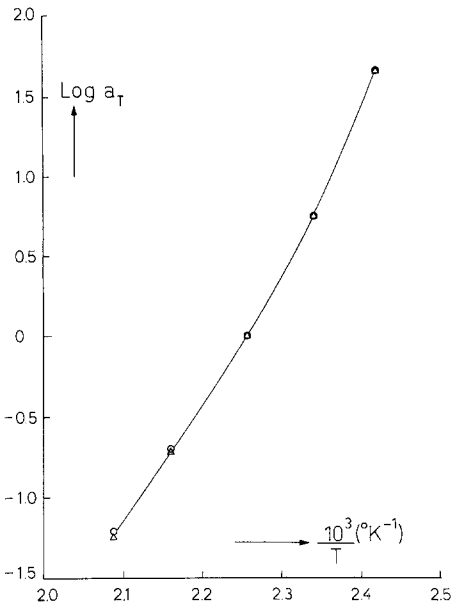

Fig. 5. The pertinent shift factor a_T as a function of the reciprocal absolute temperature as obtained by Gortemaker (3). Practically the same relation was found in the present apparatus, as presented in figure 9 of the previous paper (4)

The relaxation spectrum $H(\tau)$ appearing in eqs. [2.2] – [2.4] was replaced by the line spectrum:

$$H(\tau) = \sum_i a_i \tau_i^2 \delta(\tau - \tau_i) \qquad [4.1]$$

where the relaxation times τ_i and the weight factors $a_i = g_i/\tau_i$ are constants and δ is the Dirac's delta function. For a reference temperature of $\theta_r = 170\,°C$ the line spectrum of the investigated polystyrene melt is given by Laun et al. (11). Nine relaxation times τ_i between $5 \cdot 10^{-5}$ and 500 s at logarithmically equal distances $\Delta \ln \tau$ were chosen. The weight factors a_i were obtained from the storage and loss moduli $G'(\omega)$ and $G''(\omega)$ by a linear regression procedure. The relaxation times τ_i and the corresponding weight factors a_i and $g_i = a_i\tau_i$ are given in table 1. This line spectrum can be used in the non-linear viscoelastic model described in section 2.2 by replacing τ_i by τ_{0i} and $g_i = a_i\tau_i$ by G_{0i}.

Table 1. Line spectrum of the investigated polystyrene melt for a reference temperature of θ_r = 170°C determined by Laun et al. (11)

i	Relaxation time τ_i [s]	Weight factor a_i [Pa.s^{-1}]	Elastic modulus $g_i = a_i\tau_i$ [Pa]
1	500	$2.88 \cdot 10^{-2}$	$1.44 \cdot 10^{1}$
2	83	$2.39 \cdot 10^{0}$	$1.99 \cdot 10^{2}$
3	15	$1.68 \cdot 10^{2}$	$2.52 \cdot 10^{3}$
4	2.8	$3.43 \cdot 10^{3}$	$9.29 \cdot 10^{3}$
5	0.5	$4.91 \cdot 10^{4}$	$2.46 \cdot 10^{4}$
6	$8.3 \cdot 10^{-2}$	$4.79 \cdot 10^{5}$	$3.98 \cdot 10^{4}$
7	$1.5 \cdot 10^{-2}$	$2.48 \cdot 10^{6}$	$3.72 \cdot 10^{4}$
8	$2.8 \cdot 10^{-3}$	$1.58 \cdot 10^{7}$	$4.43 \cdot 10^{4}$
9	$5 \cdot 10^{-4}$	$2.71 \cdot 10^{8}$	$1.36 \cdot 10^{5}$

5. Performance of the measurements and results

As already mentioned in the introduction the optical and mechanical measurements are carried out simultaneously. Forces are recorded on paper as functions of time. The results of the force measurements as given in this paper are already corrected using the method described in section 3.2. In this way the time dependent rim pressure is obtained, which has been identified with the value of the normal stress. The inner cylinder used for the correction has a radius of $R_2 = 6.5$ mm. The flow birefringence is measured exactly in the centre of the gap; i.e. the light beam passes through the stagnation point perpendicular to the z-axis in figure 1. The wave length of the used light is 546.1 nm. For these measurements use has been made of an Ehringhaus compensator. Because this compensator must be operated by hand, only discrete values of Δn as a function of time are available. The time dependent measurements are carried out in the following way: the compensator is adjusted to a preselected value and the time is measured from the start of the experiment up to the moment the fringes, coming from both sides of the plane of symmetry, touch each other. This method gives nicely reproducible results.

The build-up, steady state and relaxation of the flow birefringence Δn and of the value of the tensile stress $-\sigma_{11}$ are measured at four different temperatures and several values of the extension rate $\dot{\varepsilon}$. By the use of fixed velocities of the pistons the values of the extension rate $\dot{\varepsilon}$ were the same at the four temperatures and had to be reduced to $\dot{\varepsilon} a_T$, as valid at the reference temperature $\theta_r = 170\,°C$. In table 2 the total range of values of the extension rate $\dot{\varepsilon} a_T$ at the reference temperature is given. Use has been made of the shift factor a_T shown in figure 5.

In figures 6 and 7 the flow birefringence and the rim pressure σ are plotted as functions of the time for four temperatures and a series of values of the extension rate $\dot{\varepsilon}$. From these

Table 2. Values of the reduced extension rates $\dot{\varepsilon}_0 = \dot{\varepsilon} a_T$ at the reference temperature $\theta_r = 170°C$

Temperature of the measurement θ [°C]	Pertinent shift factor a_T	Values of nominal extension rates $\dot{\varepsilon}$ [s^{-1}]					
		$-3.6 \cdot 10^{-3}$	$-4.8 \cdot 10^{-3}$	$-7.2 \cdot 10^{-3}$	$-9.6 \cdot 10^{-3}$	$-1.44 \cdot 10^{-2}$	$-1.8 \cdot 10^{-2}$
140.6	32.3	$-1.17 \cdot 10^{-1}$	$-1.56 \cdot 10^{-1}$	$-2.32 \cdot 10^{-1}$	$-3.10 \cdot 10^{-1}$	–	–
150.2	9.8	$-3.50 \cdot 10^{-2}$	$-4.70 \cdot 10^{-2}$	$-7.06 \cdot 10^{-2}$	$-9.41 \cdot 10^{-2}$	$-1.41 \cdot 10^{-1}$	$-1.76 \cdot 10^{-1}$
158.6	3.9	$-1.41 \cdot 10^{-2}$	$-1.87 \cdot 10^{-2}$	$-2.81 \cdot 10^{-2}$	$-3.75 \cdot 10^{-2}$	$-5.60 \cdot 10^{-2}$	$-7.03 \cdot 10^{-2}$
171.9	0.82	$-2.95 \cdot 10^{-3}$	$-3.93 \cdot 10^{-3}$	$-5.90 \cdot 10^{-3}$	$-7.86 \cdot 10^{-3}$	$-1.18 \cdot 10^{-2}$	–

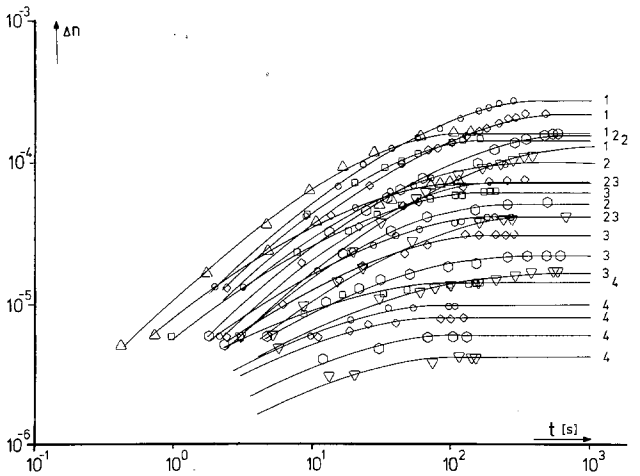

Fig. 6. The flow birefringence Δn as a function of time during the build-up experiments at four different temperatures and several extension rates. The figures at the right-side of the curves indicate the temperatures 1: 140.6°C; 2: 150.2°C; 3: 158.6°C; 4: 171.9°C. The reduced extension rates are: ▽: $-3.6 \cdot 10^{-3}$ s^{-1}, ⬡: $-4.8 \cdot 10^{-3}$ s^{-1}, ◇: $-7.2 \cdot 10^{-3}$ s^{-1}, ○: $-9.6 \cdot 10^{-3}$ s^{-1}, □: $-1.44 \cdot 10^{-2}$ s^{-1}, △: $-1.8 \cdot 10^{-2}$ s^{-1}.

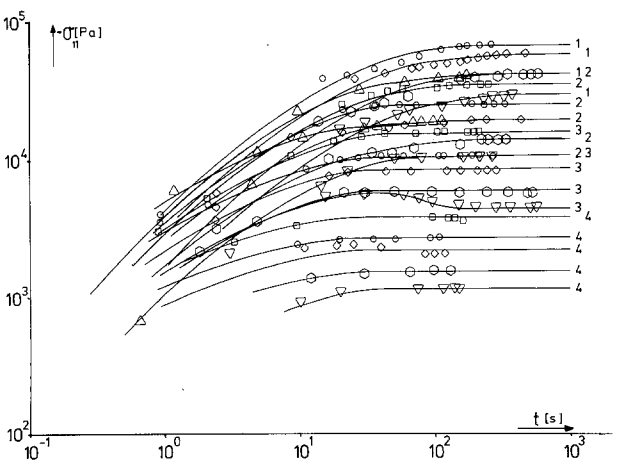

Fig. 7. The tensile stress $-\sigma_{11}$ as a function of time during the build-up experiments. The temperatures and extension rates are equal to those in figure 6

curves one can see that the rim pressure σ is always raising faster than the birefringence Δn. As mentioned before, the force measurement was recorded on paper continuously. So its was quite easy to see when the pressure reached a steady value. The flow birefringence measurements were stopped when the force became constant because there was no further significant increase of the optical signal. Measurements over a long time were not carried out because the amount of material was not sufficient for such measurements. In figure 8 time has been eliminated from the birefringence and force measurements, so that Δn is plotted as a function of the rim pressure σ for several values of the reduced extension rate $a_T\dot{\varepsilon}$. To avoid overcrowding in this figure not all the available and used measurements are drawn. The open

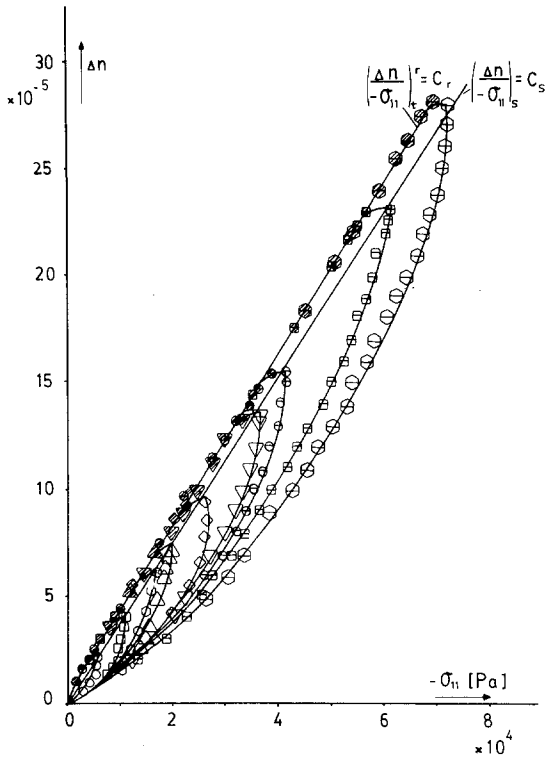

Fig. 8. The flow birefringence as a function of the tensile stress $-\sigma_{11}$. The open symbols are from the build-up phase of the experiment; the hatched symbols from the relaxation measurement. Only a few of the available measurements are shown in this figure to avoid overcrowding. The straight line through the steady state data points give a stress-optical coefficient $C_s = -3.6 \cdot 10^{-9}$ m²/N; the line through the relaxation data points gives a $C_r = -4.0 \cdot 10^{-9}$ m²/N. The reduced extension rates at a reference temperature of 170 °C are:
○: $-1.87 \cdot 10^{-2}$ s^{-1}, □: $-3.75 \cdot 10^{-2}$ s^{-1}, ⬡: $-5.60 \cdot 10^{-2}$ s^{-1}, △: $-7.03 \cdot 10^{-2}$ s^{-1}, ◇: $-9.41 \cdot 10^{-2}$ s^{-1}, ▽: $-1.41 \cdot 10^{-1}$ s^{-1}, ⊖: $-1.76 \cdot 10^{-1}$ s^{-1}, ⊟: $-2.32 \cdot 10^{-1}$ s^{-1}, ⊖: $-3.10 \cdot 10^{-1}$ s^{-1}

symbols are representing the build-up. Also here it appears that the birefringence is slower than the rim pressure. For the steady state all points $\Delta n(\sigma)$ lie on a single straight line. The slope of this line gives a value for the apparent stress-optical coefficient

$$C = \frac{\Delta n}{\sigma_{11}} = -\frac{\Delta n}{\sigma} = -3.6 \cdot 10^{-9}\,\mathrm{m^2/N}.$$

The hatched symbols in figure 8 give points from relaxation measurements. The relaxation after steady state shows the same time-dependent behaviour for the birefringence $\Delta n^r(t_1)$ and for the rim pressure $\sigma^r(t_1)$ resulting in a second straight line in figure 8. The slope of this line furnishes a value of $C = -4.0 \cdot 10^{-9}$ m²/N for the stress-optical coefficient. This value of the stress-optical coefficient is equal to the one found in shear experiments. The difference between the coefficient C obtained from the steady state measurements and from the relaxation measurements seems to be connected with a drop in the stress σ observed directly after the cessation of the extension. The relative value of this drop is the same for all measurements in spite of the different temperatures and extension rates. The difference in the time-dependent behaviour of the birefringence and the rim pressure in the build-up fase is obviously caused by undesired shear in the melt and by friction between the wall and the melt. Apparently, the optical measurements are less affected because these measurements are carried out in the plane of symmetry.

For a stressing experiment at constant $\dot{\varepsilon}$ it makes sense to speak of a total Hencky strain, of which the value increases linearly with time. In fact, assuming that $\dot{\varepsilon}$ is a constant from the moment the apparatus is started and that $\dot{\varepsilon}$ is the same in the whole sample, one can write $\varepsilon = \dot{\varepsilon} t$. This equation holds until $\varepsilon = \varepsilon_z = -2.4$ is reached. In fact, as pointed out in the previous paper, a Hencky strain of $\varepsilon_z = \ln(l/l_0) = -2.4$ can hardly be surpassed because of the fact that deformation starts only at the transition from the cylindrical to the trumpet shaped part of the duct. In figures 9 and 10 $\Delta n(\varepsilon)$ and $\sigma(\varepsilon)$ are given, as obtained from all available measurements at the four different temperatures. The theoretical limit of the Hencky strain $\varepsilon_z = -2.4$ is indicated by the dotted vertical line. The time needed to reach the steady operation of the apparatus i.e. $t = \varepsilon/\dot{\varepsilon} = 2{,}4/|\dot{\varepsilon}|$ is nicely reproduced by the mechanical measurements. On the other hand the optical measurements give the impression that at relatively high negative extension rates and relatively low temperatures the steady state is not yet reached for the fluid particles at $\varepsilon_z = -2{,}4$*).

*) In this connection it is of interest that one of the present authors has recently shown that a limit of $\varepsilon_z = -2.4$ holds only for the layers at the height of the rims of the trumpets, whereas layers closer to the plane of symmetry show values beyond -2.4. Notwithstanding the fact that for $z = 0$ the limiting value of ε_z becomes minus infinity, the average value for the material in the clearance is only -3.4 (12).

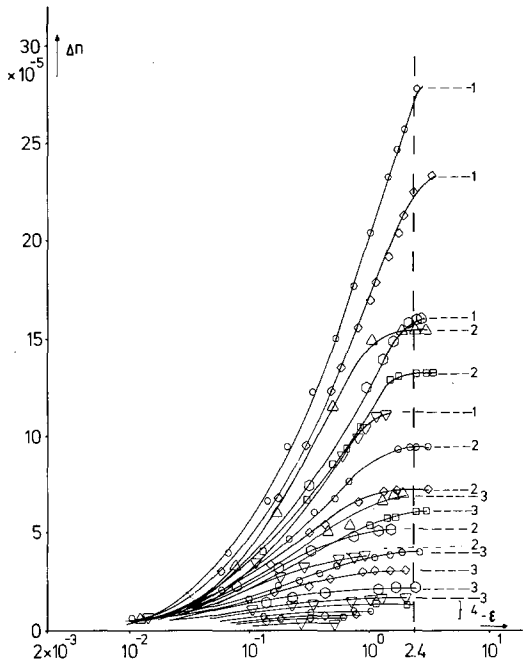

Fig. 9. The flow birefringence Δn as a function of the value of the total extension $\varepsilon = \dot{\varepsilon} t$ ($\dot{\varepsilon}$ = constant during the experiment)

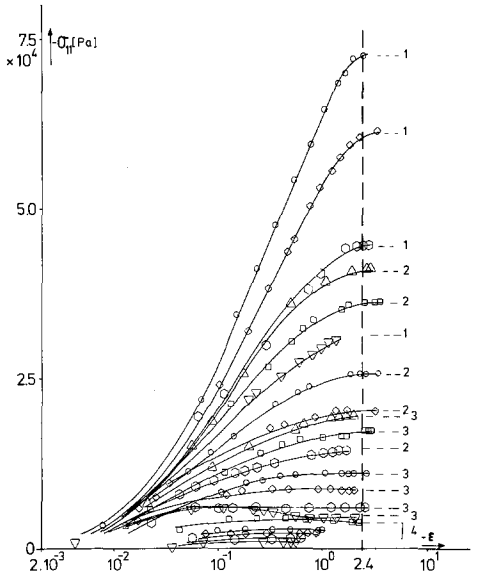

Fig. 10. The tensile stress $-\sigma_{11}$ as a function of the total extension $\varepsilon = \dot{\varepsilon} t$ ($\dot{\varepsilon}$ = constant during the experiment). The temperatures and extension rates in figures 9 and 10 are equal to those in figure 6. The dotted line at $\varepsilon_z = -2.4$ indicates the theoretical limit achievable in the apparatus

In figure 11 the extensional "stressing" viscosity as a function of time is plotted at a reference temperature of 170 °C. Only the optical

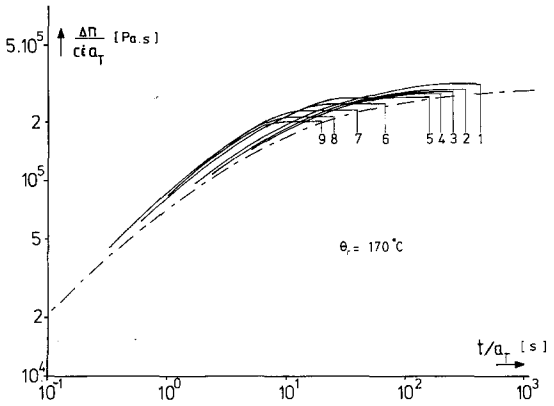

Fig. 11. The reduced extensional viscosity $\eta_e = \dfrac{\Delta n}{C\dot{\varepsilon} a_T}$ as a function of t/a_T at the reference temperature θ = 170 °C. The used temperature independent stress-optical coefficient was $C = -4.0 \cdot 10^{-9}$ m²/N. The dotted curve is calculated according to Schwarzl and Struik from eq. [2.6]. The reduced extension rates are:
1: $-2.95 \cdot 10^{-3}$ s^{-1}, 2: $-7.86 \cdot 10^{-3}$ s^{-1}, 3: $-1.28 \cdot 10^{-2}$ s^{-1}, 4: $-1.87 \cdot 10^{-2}$ s^{-1}, 5: $-3.50 \cdot 10^{-2}$ s^{-1}, 6: $-7.06 \cdot 10^{-2}$ s^{-1}, 7: $-1.17 \cdot 10^{-1}$ s^{-1}, 8: $-1.76 \cdot 10^{-1}$ s^{-1}, 9: $-3.10 \cdot 10^{-1}$ s^{-1}

measurements are used here because these measurements are assumed to be influenced to a lesser degree by the disturbance near the wall (see fig. 8). The curves in figure 11 are obtained by using the shift factor a_T from figure 5 in calculating the reduced quantities $\dot{\varepsilon}_0 = \dot{\varepsilon} a_T$ and $t_0 = t/a_T$. For the stress-optical coefficient C the value $-4.0 \cdot 10^{-9}$ m²/N was used as this value was found in previous shear experiments as well as in the present extensional relaxation experiments. (The apparent independence of C of temperature, cf. figure 8, is a peculiarity of polystyrene).

Using the method of Schwarzl and Struik, as described in section 2, an approximation of the time-dependent extensional stressing viscosity can be obtained. The storage and loss moduli $G'(\omega)$ and $G''(\omega)$ of the investigated polystyrene, known from the dynamic mechanical measurements carried out by Gortemaker (3) (see fig. 4), are used in eq. [2.6] to calculate the approximate extensional viscosity. The result of this calculation is shown in figure 11 by the dotted line. One must realize that this method is based on the idea that the fluid has a linear viscoelastic behaviour and that the calculated $\eta_e(t)$-curve is only correct for $|\dot{\varepsilon}| \to 0$. The deviation of the experimental curves from the calculated curves is obviously caused by the

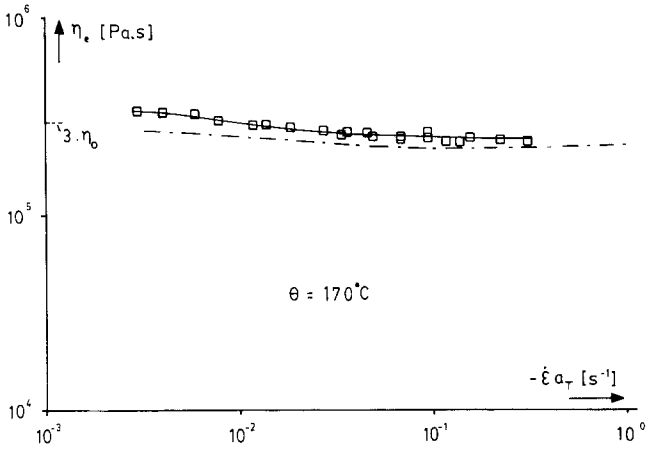

Fig. 12. The steady state extensional viscosity η_e, as calculated from birefringence measurements, is plotted as a function of the extension rate $\log(-\dot{\varepsilon}a_T)$ for Hoechst P.S. at the reference temperature of 170 °C. The dotted curve is the extensional viscosity calculated from the non-linear viscoelastic model of Acierno et al. The previously determined adjustable parameter $a = 0.35$ is used for these calculations

non-linear viscoelastic behaviour of the polystyrene melt. However, relatively small deviations from linear behaviour are also shown by Laun (13) in his mechanical extensional experiments on polystyrene (see his fig. 6).

The steady state values of $\dfrac{\Delta n}{C\dot{\varepsilon}a_T}$ are plotted in figure 12 as a function of the reduced value of the extension rate $\dot{\varepsilon}a_T$ at the reference temperature of 170 °C. The value of $C = -4{,}0 \cdot 10^{-9}$ m^2/N is used for the preparation of this figure. The pertinent values of $\dot{\varepsilon}_0 = \dot{\varepsilon}a_T$ are given in table 2. To compare the result of figure 12 with the non-linear viscoelastic model of Acierno et al., as described in section 2.2, one has to know the adjustable parameter a and the relaxation-time spectrum. De Cindio et al. (14) used this non-linear viscoelastic model to interpret transient flow birefringence measurements in shear flow for the same polystyrene. A value of $a = 0.35$, as obtained from an adaptation to the steady non-Newtonian shear viscosity, could successfully be used to describe stress growth and relaxation after different amounts of shearing. For the present calculation the continuous relaxation spectrum $H(\tau)$ used by De Cindio was replaced by the simple line spectrum given in table 1, however. From eqs. [2.15] and [2.17] the internal structural parameter x_i and the normalized i^{th} contribution to the viscosity $\eta_{e,i}/G_{0i}\tau_{0i}$ as functions of $\tau_i\dot{\varepsilon}$ can be calculated (see fig. 13). The dotted line in figure 12 gives $\eta_e = \sum_i \eta_{e,i}$ from which one can conclude that there is a fair agreement between the measured and the calculated curve. In fact, if instead of $a = 0.35$ for this parameter values 0.3 or 0.4 are used, one obtains curves which clearly deviate downward or upward from the experimental curve with increasing strain rate. For those alert readers, who will compare this figure 12 with figure 11 of the previous paper (4), the following explanation must be given for the apparent discrepancy between these figures. As a consequence of the improved method for the temperature measurement in the melt (see section 3.3) one learns that in the previous investigation

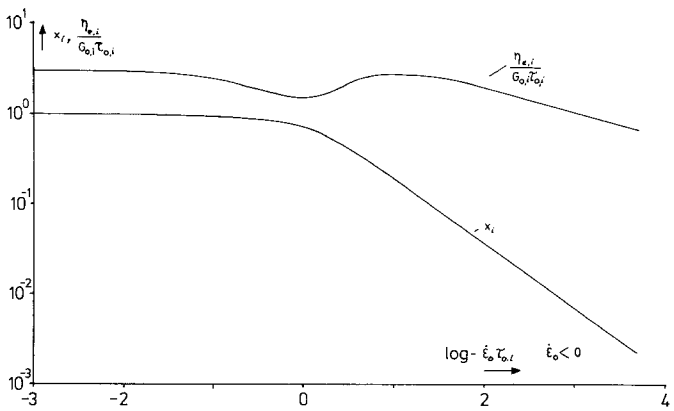

Fig. 13. The internal structural parameter x_i and the dimensionless viscosity $\dfrac{\eta_{e,i}}{G_{0i}\tau_{0i}}$ as functions of $\tau_i\dot{\varepsilon}_0$ from the Acierno theory with the adjustable parameter $a = 0.35$

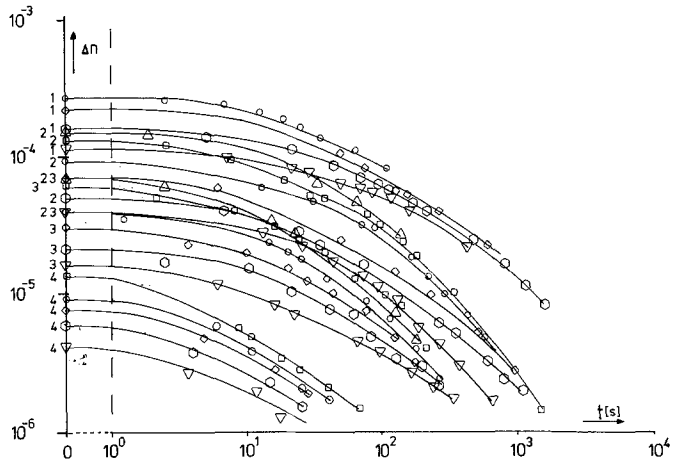

Fig. 14. The birefringence relaxation after steady state of Hoechst P.S. The figures at the left side indicate the temperatures. Temperatures and extension rates are equal to those of figure 6

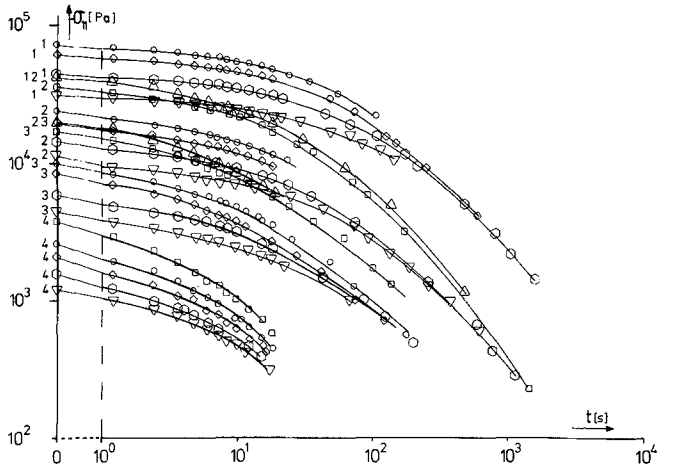

Fig. 15. The rim pressure relaxation. The temperatures and extension rates are given in figure 6

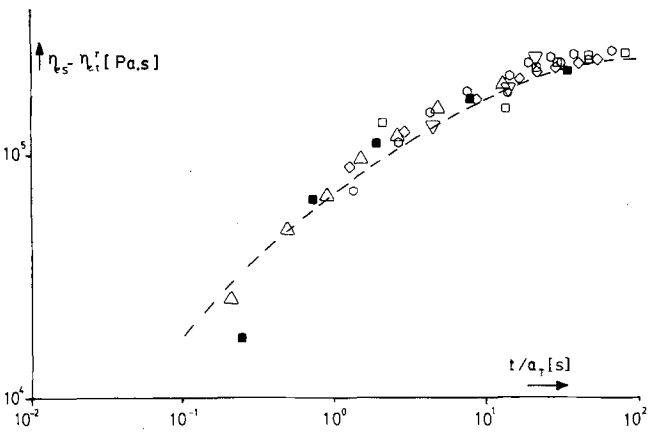

Fig. 16. A plot of $\left(\frac{\Delta n}{C\dot{\varepsilon}a_T}\right)_s - \left(\frac{\Delta n}{C\dot{\varepsilon}a_T}\right)_t^r$ and $\left[\frac{\sigma}{\dot{\varepsilon}a_T}\right]_s - \left[\frac{\sigma}{\dot{\varepsilon}a_T}\right]_t^r$ against the reduced time t/a_T at the reference temperature of 170°C. The stress-optical coefficient $C = -4.0 \cdot 10^{-9}$ m²/N is used. Previous (reduced) extension rates are:
▽: $-2.95 \cdot 10^{-3}\,s^{-1}$, ○: $-7.86 \cdot 10^{-3}\,s^{-1}$, □: $-1.18 \cdot 10^{-2}\,s^{-1}$, △: $-3.5 \cdot 10^{-2}\,s^{-1}$, ◇: $-9.4 \cdot 10^{-2}\,s^{-1}$, ⬡: $-1.15 \cdot 10^{-1}\,s^{-1}$, ■: $-1.41 \cdot 10^{-1}\,s^{-1}$.
The dashed line represents the approximation according to Schwarzl and Struik, as calculated from eq. [2.6]

measurements taken at low nominal temperatures were taken at even lower real temperatures. The apparent decrease of the steady state extensional viscosity with increasing rate of extension, as reported in the previous paper, is thus a consequence of inaccurate time-temperature shifting.

In figures 14 and 15 the relaxation of the birefringence and the rim pressure, as obtained after cessation of (nearly) steady flow, are given. The rim pressure σ shows a relatively quick drop directly after the moment that flow is stopped. This is apparently due to the already mentioned friction between the wall and the melt during the period of flow. Since the relaxing birefringence and rim pressure have, after subtraction of the initial drop in the rim pressure, the same time dependent behaviour, both data sets are used to construct figure 16. In figure 16 reduced quantities are plotted according to (a reversed) eq. [2.7]. This means that actually the stress build-up deduced from relaxation experiments is plotted. The dashed line is calculated according to Schwarzl's eq. [2.6], i.e. $[\sigma_{11}]_t/\dot{\varepsilon}$. It is inserted for comparison. The deviations from the calculated line, as must be expected in principle on account of the non-linear viscoelastic behaviour, seem to be less pronounced than in the case of the actual build-up.

6. Conclusions

Summarizing, the authors arrive at the conclusion that the performance of the proposed apparatus, which is based on the application of stagnation flow, is rather satisfactory. In particular, the flow birefringence measurements are very useful. This conclusion is based on the comparison of experimental data, as obtained in the present apparatus, with interconverted data, as calculated from dynamic mechanical measurements. In this way, evidence is obtained for the consistency of experimental data of quite different origin. Especially the compilation given in figure 11 gives rise to satisfaction. However, a serious draw back of the method seems to lie in the fact that the achievable total strain is restricted, so that the steady state situation is not easily reached. In this respect further improvements will certainly be worked out. For the purpose a larger rim diameter will be desirable. A prerequisite for the realization of this aim will be a further improvement of lubrication. Fortunately, the optical measurements are carried out with the aid of a light beam propagating along the plane of symmetry, which is rather far from the areas, where the disturbance of the ideal (flat) velocity profile occurs. Interestingly enough, the mentioned disturbances relax extremely fast. This can be concluded from the stress relaxation measurements, where a rather fast drop of the rim pressure is observed within the first second, whereas for the further relaxation, which lasts up to 10^3 s, the same time dependence is found as for the birefringence relaxation. Another argument for the correctness of the conclusion with respect to a very fast relaxation of the disturbances is furnished by the fact that the stress-optical coefficient which emerges from these extended relaxation measurements, is exactly equal to the one known from shear experiments. So one is tempted to assume that simple wall friction contributes for a great deal to the rim pressure during flow.

The steady state tensile viscosity, as determined with the aid of the optical method, can be described fairly well by the non-linear viscoelastic model of Acierno et al. For the purpose the value of the adjustable parameter found in previous shear experiments is successfully used. For $|\dot{\varepsilon}| \to 0$ this steady state tensile viscosity turns out to be equal to the well-known Trouton viscosity, which is three times the zero-shear viscosity. This, again, leads to the conclusion that the new apparatus gives reliable results, certainly as far as the optical measurements are concerned.

Acknowledgement

The present investigation has been carried out under the auspices of the Netherlands Organisation for the Advancement of Pure Research (Z.W.O.). The authors like to express their sincere thanks for this valuable support.

References

1) Janeschitz-Kriegl, H., Adv. Polymer Sci. **6**, 170 (1969).

2) Wales, J. L. S., The Application of flow birefringence to rheological studies of polymer melts. Doctoral Thesis and Monograph, Delft University Press (1976).

3) Gortemaker, F. H., A flow birefringence study of stress in sheared polymer melts. Doctoral Thesis (Delft 1976).

4) Van Aken, J. A., H. Janeschitz-Kriegl, Rheol. Acta **19**, 744 (1980).
5) Schwarzl, F. R., L. C. E. Struik, Adv. Molec. Relaxation Processes **2**, 201 (1967).
6) Wagner, M. H., Rheol. Acta **18**, 33 (1979).
7) Acierno, D., F. P. La Mantia, G. Marrucci, G. Titomanlio, J. Non-Newtonian Fluid Mech. **1**, 125 (1976).
8) Acierno, D., F. P. La Mantia, G. Marrucci, G. Rizzo, G. Titomanlio, J. Non-Newtonian Fluid Mech. **1**, 147 (1976).
9) Acierno, D., F. P. La Mantia, G. Marrucci, J. Non-Newtonian Fluid Mech. **2**, 271 (1977).
10) Gortemaker, F. H., M. G. Hansen, B. de Cindio, H. M. Laun, H. Janeschitz-Kriegl, Rheol. Acta **15**, 256 (1976).
11) Laun, H. M., M. H. Wagner, H. Janeschitz-Kriegl, Rheol. Acta **18**, 615 (1979).
12) Janeschitz-Kriegl, H., in preparation.
13) Laun, H. M., in: G. Astarita, G. Marrucci, L. Nicolais (eds.), Rheology (Proceedings of the 8th International Congress on Rheology, Naples), Vol. 2, pp. 419, Plenum Press (New York and London 1980).
14) De Cindio, B., D. Acierno, F. H. Gortemaker, H. Janeschitz-Kriegl, Rheol. Acta **16**, 484 (1977).
15) Hsu, T., P. Shirodkar, R. L. Laurence, H. H. Winter, in: G. Astarita, G. Marrucci, L. Nicolais (eds.), Rheology (Proceedings of the 8th International Congress on Rheology, Naples), Vol. 2, pp. 155, Plenum Press (New York and London 1980).

Authors' addresses:

Dr. ir. J. A. van Aken
Centre for Fire Prevention TNO
Postbus 4g
NL-2600 AA Delft

Prof. Dr. H. Janeschitz-Kriegl
Johannes-Kepler-Universität
Altenberger Straße 69
A-4040 Linz